Study with Magnetic Property Measurement of Soft Magnetic Composite Material and Its Application in Electrical Machines

Jian Guo Zhu and YouGuang Guo
Center for Electrical Machines and Power Electronics, Faculty of Engineering
University of Technology, Sydney
New South Wales, Australia
joe@eng.uts.edu.au, youguang@eng.uts.edu

Abstract— **This paper reports our study with the magnetic property measurements of soft magnetic composite (SMC) materials under both alternating and rotational magnetic excitations, and development of different electrical machines with SMC cores and three-dimensional magnetic field, such as claw pole and transverse flux motors. Three-dimensional finite element electromagnetic field analysis is conducted for determining some important parameters and optimizing the machine structures. The analysis methods are validated by the experimental results on two SMC motor prototypes.**

Keywords-soft magnetic composite; claw pole motor; transverse flux motor; finite element analysis

I. INTRODUCTION

The new soft magnetic composite (SMC) materials possess a number of advantages over the traditional laminated steels commonly used in electromagnetic devices, such as isotropic magnetic and thermal properties, very low eddy current loss and relatively low total core loss at medium and high frequencies, and nearly net-shape low cost fabrication process with good tolerance and surface finish by using well developed powder metallurgical techniques. It is anticipated that the application of SMC may lead to a revolutionary development in the manufacturing industry of electrical machines [1-3].

The basis for the material is the bonded iron powder of high purity and compressibility. The powder particles are bonded with a coating of an organic material, which produces high electrical resistivity. The coated powder is then pressed into a solid material using a die and finally heat treated to anneal and cure the bond.

This type of material is in general magnetically isotropic due to its powdered nature and this opens up crucial design benefits. The magnetic circuits can be designed with three-dimensional (3D) flux paths and radically different topologies can be exploited to obtain high motor performances, as the magnetic field restraints of lamination technology can be ignored.

Since the iron particles are insulated by the surface coating and adhesive, which is used for composite bonding, the eddy current loss is much lower than that in laminated steels, especially at higher frequencies. The total loss is dominated by hysteresis loss, which is higher than that of laminated steels due to the particle deformation during compaction. For example, at the power frequency of 50 Hz and the flux density of 1.5 T, the total core loss in SOMALOY™ 500 (with 0.5% Kenolube), a new soft magnetic composite developed recently by Höganäs AB, Sweden, is 14 W/kg [4], double that of even the low grade Kawasaki 65RM800 (0.65 mm thick, 28 x 10^{-8} Ωm) [5]. When the excitation frequency increases, however, the increment of core loss in SMC is smaller than that in electrical steels due to the much smaller eddy currents. At 400 Hz and 1.5 T the total core loss in SOMALOY™ 500 is 120 W/kg, the same as the low-medium grade Kawasaki 50RM700 (0.5 mm thick, 28 x 10^{-8} Ωm). High grade Kawasaki 35RM270 (0.35 mm thick, 54 x 10^{-8} Ωm) has one third the loss then, i.e. 40 W/kg at 400 Hz and 1.5 T. Thus, SMC materials are more likely to be better used for motors operating at higher excitation frequencies, but they are not yet as good as high grade laminations at low and medium frequencies and any superior performance must come from exploring 3D flux motor topologies, high performance drive techniques, and some other SMC features.

The utilization of SMC offers a prospect of large volume manufacturing of low cost motors. Because the iron cores and parts can be pressed in a die into the desired shape and dimensions, the further machining is minimized and hence the production cost can be greatly reduced.

To investigate the application potential of SMC materials in electrical machines, some researchers, such as those in the University of Newcastle upon Tyne, UK [2-3], Aachen University, Germany [6], University of Laval, Canada [7-9], and our research group in the Center for Electrical Machines and Power Electronics, University of Technology, Sydney (UTS), Australia [10-14], have been working in this field for a few years and the results appear to be promising.

Besides the favorable properties mentioned above, the SMC materials have also some disadvantages that should be carefully considered in the design, manufacturing and

 0-7803-8486-5/04/$20.00 © 2004 IEEE

application of electrical machines. The permeability of SMC material is significantly lower than that of electrical steels because it has less full density. Best figures are in the range of 500 for maximum relative permeability [4]. Therefore, it is expected that this material would be appropriate for construction of permanent magnet (PM) motors for which the magnetic reluctance of the magnet dominates the magnetic circuit, making such motors less sensitive to the permeability of the core than armature magnetized machines, such as induction and reluctance machines.

Because of the significant differences in magnetic, thermal, and mechanical properties, simply replacing the existing laminated iron core in an electrical machine with an SMC material will result in a loss of performance with very small compensating benefits. To fully take advantages of the SMC material and overcome its disadvantages, a great amount of research work is required on a better understanding of the material properties, novel motor topologies, advanced field analysis, design and optimization techniques, and appropriate power electronic drive system.

This paper presents our investigations on SMC's magnetic properties and its application in 3D flux PM machines. To obtain a deep understanding of the magnetic properties of SMC materials and necessary data for the design and performance analysis of SMC motors, B-H curves and core losses in square SMC samples were measured with different flux patterns (circularly and elliptically rotational and alternating) and different frequencies [10-11].

Taking into account the unique properties of the material, two SMC motors, namely a three-phase three-stack claw pole PM SMC motor and a three-phase three-stack PM transverse flux SMC motor, were designed and manufactured [12-14]. Rough and quick designs were conducted by using the equivalent magnetic circuit method, and then further refined by the 3D finite element magnetic field analysis. The performance optimization was achieved by varying certain parameters such as the magnet length to find the minimum ratio of the overall material cost over the electromagnetic torque. A number of analysis methods were developed and applied, such as the parameter calculation, core loss analysis and thermal analysis. The design and performance analysis method has been validated by the experimental results on the prototypes. Compared to the previous work [10-14], this paper presents a thorough picture of our research work on development of SMC motors and adds more updated theoretical and experimental results.

II. Measurement of Magnetic Properties of SMC

In design and simulation of electrical machines, it is necessary to properly model the properties of magnetic materials with different magnetic field excitations, such as the relation between magnetic flux density B and magnetic field strength H and core losses, in order to predict the machine performance correctly.

A square sample single sheet tester was used to measure the magnetic properties of SMC materials under two-dimensional (2D) magnetic excitations [10,11]. This tester is supported by a computerized digital signal processing system, and can measure B-H relationships and core losses with either alternating fluxes in any specified orientation or circular or elliptical rotating fluxes with any specified axis ratio. Fig. 1 illustrates schematically the testing system.

An SMC sample of 50x50x1.27 mm^3 has been systematically tested under various alternating flux densities, and circular and elliptical flux densities, rotating in the clockwise and anti-clockwise directions at frequencies of 5, 10, 20, 30, 40, 50 and 100 Hz, respectively. For example, Fig. 2 shows the measured B-H loops under 50 Hz sinusoidal alternating **B**, and Fig. 3 shows the circular **B** loci and the corresponding **H** loci.

The local flux density patterns within an electrical machine might be very complicated. The flux density locus at one location can be alternating (1D) with or without harmonics, 2D or even 3D rotating with purely circular or elliptical patterns. Experiments on samples have shown significant differences between the core losses caused by an alternating and a rotating magnetic field.

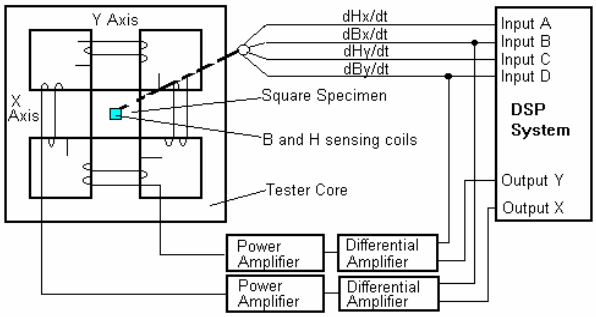

Figure 1. Schematic illustration of block diagram of the rotational **B-H** relation and core loss testing system at UTS

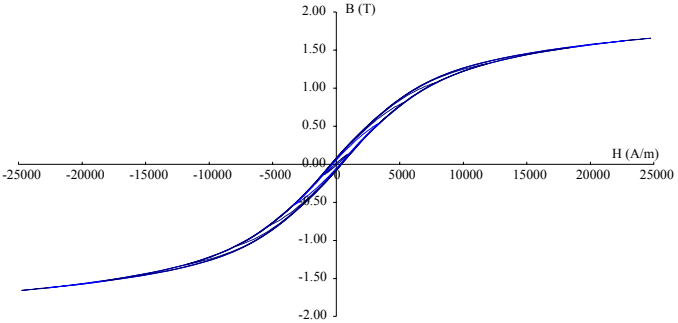

Figure 2. B-H loops under 50Hz sinusoidal alternating B

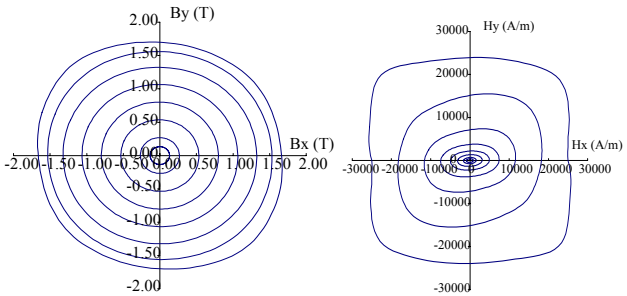

Figure 3. Loci of **B** and **H** under circular flux density at 50Hz

An improved method was outlined in [11] for calculating the core losses in 3D magnetic flux SMC machines by using 3D finite element analysis of magnetic field. The total core loss is computed by summing up the core loss of each element, which can be obtained by calculating separately the hysteresis (alternating and rotational, both purely circular and elliptical), eddy current, and anomalous losses, when the rotor rotates. The coefficients for each loss component are determined by a loss separation procedure and the experimental data obtained by using the single-sheet 2D core loss testing system.

III. CLAW POLE MACHINE

A. Structure and Dimensions

Electrical machines with claw pole rotors or stators have been manufactured in mass production for many years. These machines have quite simple excitation coil and pole systems producing the excitation magnetic fields. They are capable of producing power densities up to three times greater than conventional machines because the topology allows the pole number to be increased without reducing the magnetomotive force per pole. The excessive eddy currents in the commonly used solid steel core, however, limit the motors to very small sizes and/or low speeds and result in low efficiency.

Because of the complex structure, it is very difficult to construct the claw poles using electrical steel laminations. SMC materials offer an opportunity to overcome these problems. Fig. 4 illustrates the magnetically relevant parts of the rotor and the stator of a claw pole SMC motor prototype [14]. Table 1 lists the dimensions and major parameters. The three phases of the motor are stacked axially with an angular shift of 120° electrical from each other. Each stator phase has a single coil around an SMC core, which is molded in two halves. The outer rotor comprises a tube of mild steel with an array of magnets for each phase mounted on the inner surface. Mild steel is used for the rotor because the flux density in the yoke is almost constant.

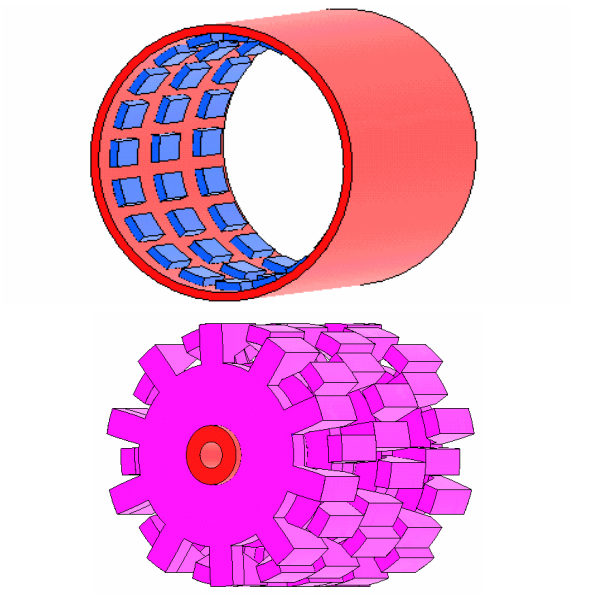

Figure 4. The magnetically relevant parts of claw pole motor

TABLE I. DIMNESIONS AND PARAMETERS OF CLAW POLE MOTOR

Dimensions and parameters	Quantities
Rated frequency (Hz)	300
Number of phases	3
Rated power (W)	500
Rated line-to-neutral voltage (V)	64
Rated phase current (A)	4.1
Rated speed (rev/min)	1800
Rated torque (Nm)	2.65
Rated efficiency (%)	81
Rated temperature in winding (°C)	115
Number of poles	20
Stator core material	SMC
Stator outer diameter (mm)	80
Effective stator axial length (mm)	93
Total motor length (mm)	137
Rotor outer diameter (mm)	94
Rotor inner diameter (mm)	82
Permanent magnets	NdFeB
Number of magnets	60
Magnet dimensions	OD88 x ID82 x 15 mm arc 12°
Magnetization direction	Radial
Main airgap length (mm)	1
Sub-airgap length* (mm)	4.2
Stator shaft material	Mild steel
Number of coils	3
Coil window dimension (mm^2)	17 x 11
Number of turns	75
Number of strands	2
Diameter of copper wire (mm)	0.71
Resistance per phase at 115°C (Ω)	0.302

* The sub-airgap is defined as the gap between the sides of the claw poles of the two separated discs.

B. 3D Numerical Field Analysis

It is evident that the complicated shape of a claw pole machine leads to a truly 3D magnetic flux. Therefore, it is absolutely necessary that 3D finite element analysis (FEA) be conducted for accurate determination of the parameters and performance of the electrical machine.

The magnetic circuits of three stacks (or phases) of the motor are basically independent. For each stack, because of the symmetrical structure, it is only required to analyse the magnetic field in one pole pitch, as shown in Fig. 5.

At the two radial boundary planes, the magnetic scalar potential used to solve the magnetic field distribution obeys the so-called half-periodical boundary conditions:

$$\varphi_m(r, \Delta\theta/2, z) = -\varphi_m(r, -\Delta\theta/2, -z) \quad (1)$$

where $\Delta\theta = 18^\circ$ is the angle of one pole pitch.

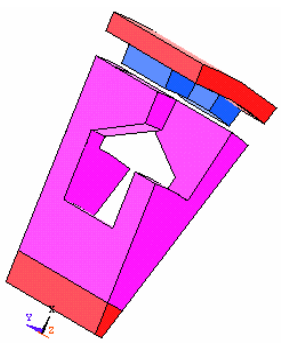

Figure 5. Region for field solution

1) No-load magnetic field calculation at $\theta = 0^o$: Rotor position $\theta = 0^o$ is defined as when the magnets share the same axes as the stator claw poles respectively. When the rotor is at the position of 0^o, the main magnetic circuit has the highest permeance and the stator winding links the maximum magnetic flux. The no-load magnetic field distribution is calculated to find out the magnetic flux linking the stator winding. The motor structure should be adjusted such that the flux linkage of the stator winding is the maximum (assuming that the flux waveform varies little and so its amplitude is representative). Fig. 6 illustrates the flux density vectors with line lengths proportional to the magnitudes.

2) No-load flux and back electromotive force: As the rotor rotates, the flux linking the stator winding varies and an electromotive force (*emf*) is induced. The *emf* frequency depends on the rotor speed, while the *emf* waveform is determined by the waveform of the flux. At no-load, the flux waveform was calculated by rotating the rotor magnets for one pole pitch in 12 steps. As plotted in Fig. 7, this flux waveform is almost perfectly sinusoidal versus the rotor position.

3) Cogging torque: Fig. 8 shows the cogging torque versus the rotor position for one stack of the machine, calculated by the Coulomb virtual work method. This curve was calculated by rotating the rotor for one pole pitch in 12 steps, i.e. 15^o electrical per step.

The harmonics of the cogging torque can be obtained by applying the discrete Fourier transform (DFT). Since the cogging torque has a period of 180^o electrical and anti-symmetry about zero, it contains only even sine harmonics. The cogging torque harmonics of phase *A* was obtained by the DFT method as following

$$T_A \approx 0.6150\sin 2\theta + 0.0629\sin 4\theta - 0.1270\sin 6\theta - 0.0479\sin 8\theta + 0.0030\sin 10\theta + 0.0001\sin 12\theta \quad (2)$$

where θ is the rotor angle in electrical degrees. Because the three stacks are shifted by 120^o electrical, all harmonics other than the 6th and its multiples cancel each other, and the resultant cogging torque can be expressed as

$$T_{cog} = T_A + T_B + T_C \approx -0.3810\sin 6\theta + 0.0003\sin 12\theta \quad (3)$$

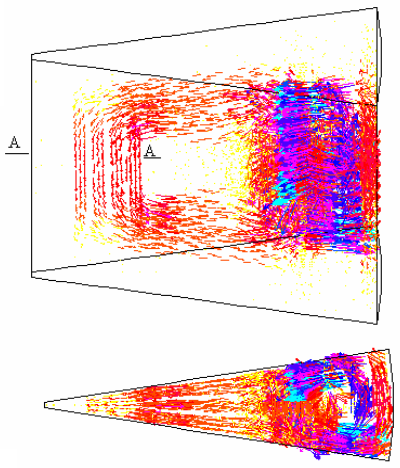

Figure 6. Vector plot of no-load flux density

4) Core losses: The core loss is calculated by the improved method as explained in [11]. Fig. 9 plots the calculated and the measured core losses of the motor at different speeds at no-load. It can be seen that the theory agrees well with the experiment.

Core losses do occur in the magnets and the rotor yoke due to the ripples of flux density when the rotor rotates. However, the numerical results of FEA of the magnetic field have shown that the flux density vectors in the magnets and the rotor yoke are nearly constant and the ripples are negligible. Therefore, only the power loss in the SMC stator core was computed.

Under load operation, the magnetic field in the core is produced by not only the rotor magnets, but also the stator current, which can be very different from that at no-load. The calculation of core loss with load uses the similar procedure as for calculating the no-load core loss, except that the magnetic field analysis was conducted with both the stator current and PM excitations.

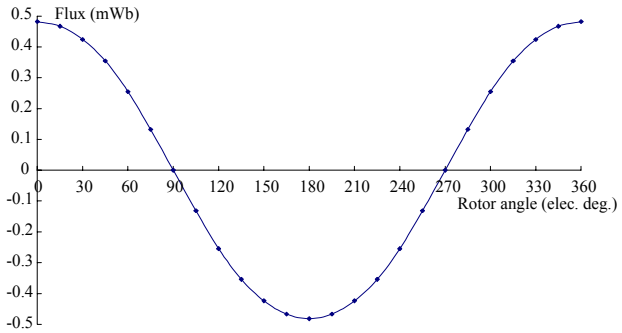

Figure 7. Per turn no-load flux of a phase winding

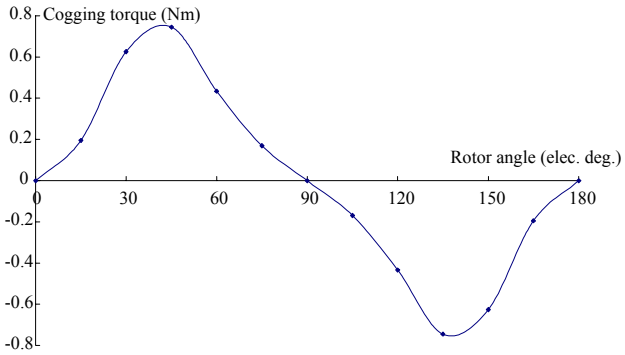

Figure 8. Cogging torque versus rotor position for one stack

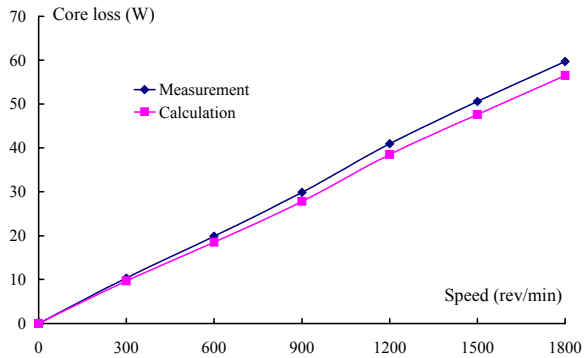

Figure 9. Core loss calculation and measurement at no-load

5) Inductance and armature reaction: The self-inductance of each phase winding can be calculated by

$$L_1 = \frac{N_1 \phi_1}{I_1} \tag{4}$$

where ϕ_1 is the magnitude of the flux linking the stator winding due to a stator current I_1 in each of N_1 turns. The flux can be obtained from the results of a field analysis with a stator current I_1 while the PMs are "switched off", i.e. remanence is set to zero. From Table II, it can be seen that the per-turn inductance is very uniform against the rotor angle. The self-inductance is deduced as 5.24 mH for 75 turns as it is proportional to the square of number of turns. It is also shown in Table II that the armature reaction for rated current is quite small and it will not demagnetise the magnets.

TABLE II. INDUCTANCE AND AMATURE REACTION IN MAGNETS

Rotor position (elec. deg.)	Self inductance per turn (μH)	Maximum B in magnets (T)
0	0.932	0.031
45	0.932	0.030
90	0.932	0.037

C. Performaance Calculation

1) Stator winding resistance: The resistance of the stator winding can be calculated by

$$R_1 = \frac{\rho l_1}{A_1} \tag{5}$$

where l_1 is the total wire length in m, A_1 the wire cross sectional area in m^2, and ρ the electrical resistivity in Ωm of the stator winding.

2) *Stator winding reactance*: The synchronous reactance is calculated by

$$X_1 = 2\pi f_1 L_1 \tag{6}$$

where f_1 is the operating frequency and L_1 is the synchronous inductance of the stator winding in Henry. In the case of this three-phase three-stack motor, L_1 equals the self-inductance of the stator winding.

3) *Power, torque and efficiency*: When the current I_1 is controlled in phase with the induced *emf*, E_1 in the stator winding, the achievable maximum electromagnetic power P_{em} is

$$P_{em} = 3E_1 I_1 \tag{7}$$

The output power, output torque, input power, and efficiency can be calculated by

$$P_{out} = P_{em} - P_{Fe} - P_{mec} \tag{8}$$

$$T_{out} = P_{out} / \omega_r \tag{9}$$

$$P_{in} = P_{em} + P_{cu} \tag{10}$$

$$P_{cu} = 3I_1^2 R_1 \tag{11}$$

$$\eta = P_{out} / P_{in} \tag{12}$$

where P_{Fe} is the core loss, P_{mec} the mechanical loss, P_{cu} the copper loss, and ω_r the rotor angular speed in mechanical rad/s.

4) *Inverter input voltage and current*: The line-to-neutral *rms* voltage and phase *rms* current have the following relationship when the motor is under the optimum brushless DC control:

$$V_1 = \sqrt{(E_1 + I_1 R_1)^2 + (I_1 X_1)^2} \tag{13}$$

The corresponding DC input voltage of the inverter can be approximately estimated by

$$V_{DC} = 2.34 V_1 \tag{14}$$

though this is only accurate for no-load [15]. If PWM is not used in the inverter, and switching takes place at the optimum time, the mean DC supply current I_{DC} is related approximately to the AC line *rms* fundamental current I_1 by [15]

$$I_{DC} = (1.0 \sim 1.28) I_1 \tag{15}$$

The coefficient depends on the load and other factors such as current waveform.

5) *Thermal analysis*: To obtain an economic utilization of the materials and safe operation of the motor it is necessary to predict with reasonable accuracy the temperature rise of the internal parts, especially in the coils and magnets. In this paper, the temperature rise is calculated by using a hybrid thermal model with distributed heat sources. Fig. 10 shows the schematic diagram of thermal network. For higher computation accuracy, any part, e.g. the SMC stator claw pole, can be divided into many small segments.

D. Prototype Experiment

1) Resistance measurement: When a fixed DC current of 1 A is fed into any two-phase windings in series via a DC power supply device, the voltage across the terminals are measured as 0.440 V, so the phase resistance is 0.22 Ω at room temperature. The resistance at the rated temperature can be predicted as 0.302 Ω by

$$R_{t2} = R_{t1} \frac{234.5 + t_2}{234.5 + t_1} \tag{16}$$

where t_1 is the room temperature of 20 °C, and t_2 the rated operating temperature of 115 °C. The measurement agrees with the calculation very well.

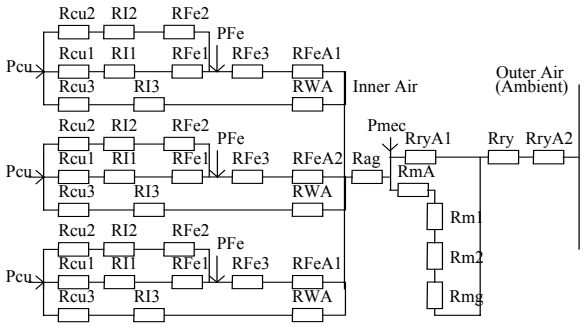

Figure 10. A schematic diagram of thermal network

2) *Inductance measurement*: The stator phase winding inductance was measured by applying a 50Hz AC voltage across two terminals of the three phase winding, $2V_{ac}$, and measuring the current flowing through the windings, I_{ac}, when the rotor is locked. The inductance can then be calculated as

$$L_1 = \frac{\sqrt{(V_{ac} / I_{ac})^2 - R_1^2}}{2\pi f_1} \quad (17)$$

where R_1 is the resistance of a phase winding.

The measured phase inductance is 5.79 mH, which is in a good agreement with the prediction by magnetic field analysis.

3) *Cogging torque measurement*: For the measurement of cogging torque, the stator is mounted on a rotatable air-bearing plate with very little mechanical friction, as shown in Fig. 11. By displacing the stator with the rotor fixed, the cogging torque was measured and plotted in Fig. 12. It substantially matches the theoretical calculation.

4) Steady state characteristics: The motor is operated with a DC/AC inverter and a sensorless brushless DC controller. Fig. 13 shows the test rig of the 3-phase 3-stack claw pole PM SMC motor (on the right). A printed circuit disc armature DC machine (on the left) is connected via a torque transducer (in the middle) as the load when the prototype is operated as a motor, or the driver when the prototype is operated as a generator.

The steady state characteristics were measured with different loads at a fixed inverter DC link voltage. The load was varied by changing the electrical output of the DC generator. Fig. 14 shows the mechanical characteristic with the fixed DC link voltage, 165V, and Fig. 15 plots the variations of the input power, output power and efficiency against the output torque.

Figure 11. Cogging torque test set-up of the claw pole SMC motor

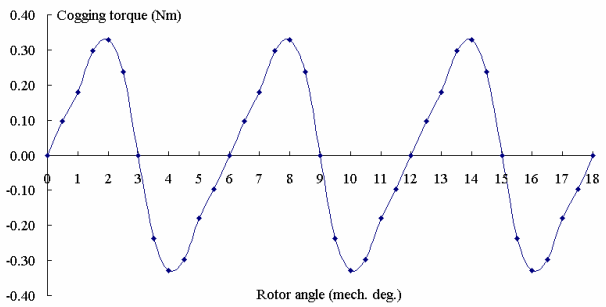

Figure 12. Measured cogging torque of the claw pole SMC motor

5) *Measurement of back emf waveform*: When the prototype operates as a generator, driven by the DC machine, the back electromotive force can be measured from the open circuit voltage. Fig. 16 shows the measured *emf* waveforms, which are very close to sinusoidal. The waveforms of three phases are with the same magnitude but shifted each other by 120 electrical degrees in phase angles.

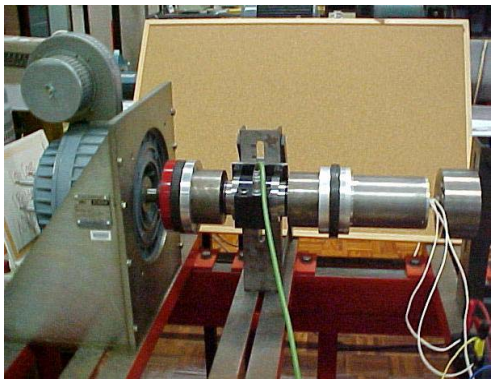

Figure 13. Test rig of the claw pole PM motor with SMC stator

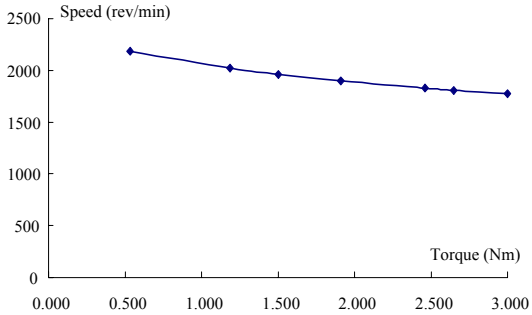

Figure 14. Curve of speed against output torque

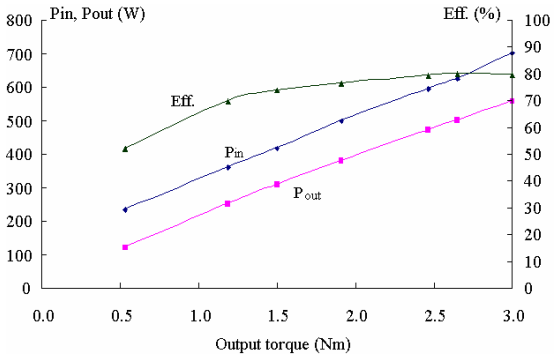

Figure 15. Curves of inverter input power, motor output power and efficiency versus output torque

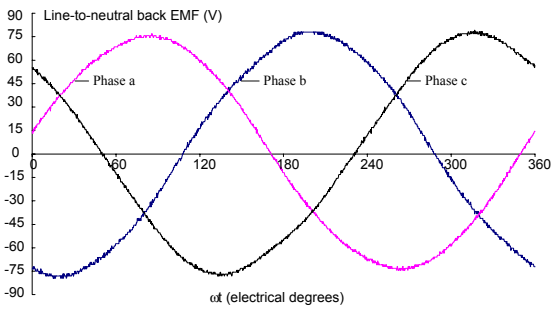

Figure 16. Measured back *emf* waveforms at 1800 rpm

6) Core loss measurement: The core loss is measured by separating the core loss from the mechanical loss using the dummy stator method, which includes two measurements. In the first measurement, the prototype is driven by the DC motor on the left and the power fed into the DC motor is measured. The second measurement is conducted while the SMC stator of the prototype is replaced by a wood tube.

The difference between the readings of electromagnetic power for the two cases gives the core loss, as illustrated in Fig. 9. Here, we assumed the core loss and mechanical loss of the DC driving motor are constant at certain rotor speed. The dummy stator is used to simulate the windage. The prototype is assumed to have the same windage and friction loss for the SMC stator and the dummy stator if it is driven at the same speed.

7) Measurement of temperature rise: The winding temperature is measured by the resistance method, comparing the resistance R_{t1} at room temperature t_1 and the measured resistance R_{t2} immediately after the load test. Since the thermal time constant is quite large, the winding temperature will not drop very quickly.

$$t_2 = \frac{R_{t2}}{R_{t1}}(234.5 + t_1) - 234.5 \ ^{o}\mathrm{C} \qquad (18)$$

The temperature measured by this method is the average of the winding and was checked by thermocouples embedded in the stator windings. A factor needs to be added for the hottest spot. To detect the rotor yoke temperature, an infrared temperature probe is used.

E. Comparison with Laminated Motors

Since it givens the rated performance of 500 W output, 1800 rpm, 81% efficency, the designed claw pole SMC motor with outer diameter (OD) of 94 mm and an axial length (excluding shaft) of 137 mm compares favourably with other laminated motors. For example, an aluminum TEFV induction motor rated 370 W at 1380 rpm, which is about the same torque (3% lower), has an efficiency of only 73% from frame size D71G, with an OD of 126 mm including fins and total length of 220 mm (including fan but excluding shaft) [16]. As a second comparison – a lower torque but higher power (610 W) brushless DC servo motor, rated 2.2 Nm with locked rotor and 1.95 Nm at 300 rpm (when mounted to a cooled 25 ^{o}C flange), has square cross-section 100 mm and a length of 173 mm [17]. The claw pole SMC motor has similar performance from a smaller volume compared to these commercial motors.

IV. TRANSVERSE FLUX MOTOR

To further investigate the potential of SMC materials in manufacturing of small motors with complex structures, a three-phase three-stack PM transverse flux motor has also been designed, fabricated and tested. The transverse flux and the claw pole machines are very close in many aspects, and thus the parameter calculation and performance prediction in the design of the two prototypes can follow the similar procedure, as described in the last section.

The magnetically relevant parts of the TFM motor are shown in Fig. 17, and the dimensions and major parameters are listed in Table III.

The prototype has been extensively tested and the experiment results match the calculated values. As an example, the measured mechanical characteristics with different inverter DC link voltages are shown in Fig. 18.

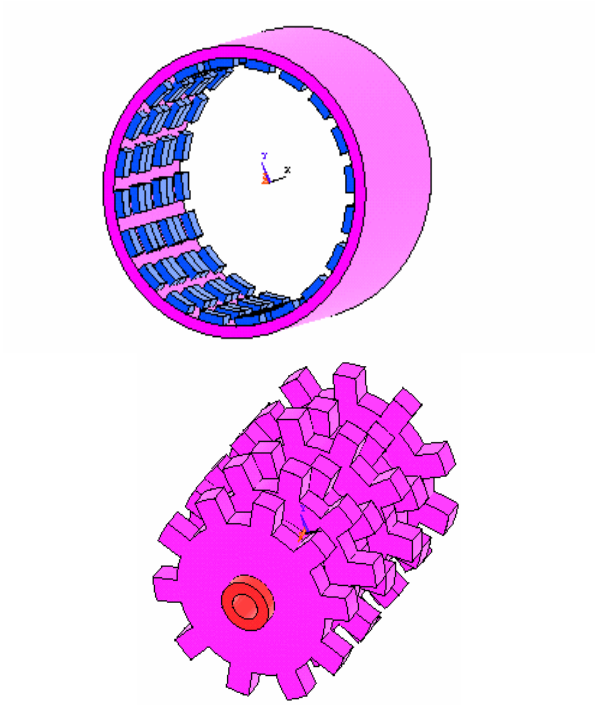

Figure 17. Magnetically relevant parts of the TFM prototype

TABLE III. DIMENSIONS AND PARAMETERS OF THE TFM MOTOR

Dimensions and parameters	Quantities
Rated frequency (Hz)	300
Number of phases	3
Rated power (W)	640
Rated line-neutral voltage (V)	80
Rated phase current (A)	5.5
Rated speed (rev/min)	1800
Rated torque (Nm)	3.4
Rated efficiency (%)	79.5
Rated winding temperature rise (^{o}C)	90
Number of poles	20
Stator core material	SOMALOY™ 500
Stator outer radius (mm)	40
Effective stator axial length (mm)	93
Rotor outer radius (mm)	47
Rotor inner radius (mm)	41
Permanent magnets	NdFeB, Grade N30M
Number of magnets	120
Magnet dimensions	OD88 x ID82 x 9 mm arc 12^{o}
Magnetisation directions	Radially outward or inward
Main airgap length (mm)	1
Stator shaft	Mild steel
Shaft outer radius (mm)	9.5
Number of coils	3
Coil window dimension (mm^2)	15 x 20.5
Number of turns	125
Number of strands	1
Diameter of copper wire (mm)	1.25

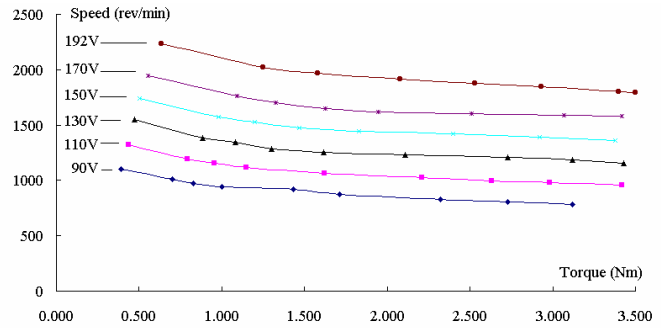

Figure 18. Curves of the speed against output torque with different inverter DC link voltages

The TFM prototype is designed to have the same main sizes as the claw pole prototype. The transverse flux motor, however, uses 20% more permanent magnets and twice as much copper material, and can produce 28% more electromagnetic power at a given rotor speed. It should be noted that using the double-sided flux concentration in TFM would produce a higher specific power or torque [18]. In this paper, the single-sided surface-mounted PM type was chosen for simple fabrication, but still produced almost twice power as that of an induction motor with similar volume.

V. CONLUSION

To investigate the application SMC materials in electrical machines, the magnetic properties of SMC have been tested with different excitations, and a 3-phase PM claw pole motor with SMC core and a 3-phase PM SMC transverse flux motor have been designed and manufactured. The prototypes are operated with a sensorless brushless DC drive and their performance is comparable to that of similar motors with electrical steel cores at potentially reduced manufacturing cost. The method for the motor design and performance analysis has been validated by experiment.

ACKNOWLEDGMENT

The authors wish to thank Höganäs AB, Sweden, for supplying preforms of SOMALOY™ 500.

REFERENCES

[1] "The latest development in soft magnetic composite technology, from Högnäs Metal Powders," Reports of Högnäs AB, Sweden, 1997-2003.

[2] A.G. Jack, "Experiences with the use of soft magnetic composites in electrical machines," Proc. Int. Conf. on Electrical Machines, Istanbul, Turkey, Sept. 1998, pp. 1441-1448.

[3] T.J. Hammons, H.B. Ertan, J.A. Tegopoulos, W. Drury, M. Ehsani, T. Nakata, and A.G. Jack, "1998 ICEM review," IEEE Power Engineering Review, Feb. 1999, pp. 12-17.

[4] "Soft magnetic composites from Höganäs Metal Powders - SOMALOY™ 500," Höganäs Manual, 1997.

[5] "RM-core non-oriented magnetic steel sheet and strip," Catalogue, Kawasaki Steel, March 1999.

[6] R. Blissenbach, G. Henneberger, U. Schäfer, and W. Hackmann, "Development of a transverse flux traction motor in a direct drive system," Proc. Int. Conf. on Electrical Machines, Helsinki, Finland, 2000, pp. 1457-1460.

[7] J. Cros, P. Viarouge, and A. Halia, "Brushless DC motors with concentrated windings and soft magnetic composites armatures," Proc. IEEE IAS Annual Meeting, Chicago, USA, 2001, pp. 2549-2556.

[8] J. Cros and P. Viarouge, "New structures of polephase claw-pole machines," IEEE Trans. Ind. Applicat., Vol. 40, Jan./Feb. 2004, pp. 113-120.

[9] J. Cros, P. Viarouge, Y. Chalifour, and J. Figueroa, "A new structure of universal motor using soft magnetic composite," IEEE Trans. Ind. Applicat., Vol. 40, Mar./Apr. 2004, pp. 550-557.

[10] J.G. Zhu, J.J. Zhong, V.S. Ramsden, and Y.G. Guo, "Power losses of composite soft magnetic materials under two dimensional excitations," J. Applied Physics, Vol. 85, April 1999, pp. 4403-4405.

[11] Y.G. Guo, J.G. Zhu, J.J. Zhong, and W. Wu, "Core losses in claw pole permanent magnet machines with soft magnetic composite stators," IEEE Trans. Magn., Vol. 39, Sept. 2003, pp. 3199-3201.

[12] Y.G. Guo, J.G. Zhu, P.A. Watterson, and W. Wu, "Comparative study of 3D flux electrical machines with soft magnetic composite core," IEEE Trans. Ind. Applicat., Vol. 39, Nov./Dec. 2003, pp. 1696-1703.

[13] Y.G. Guo, J.G. Zhu, P.A. Watterson, and W. Wu, "Design and analysis of a transverse flux machine with soft magnetic composite core," Int. Conf. Elec. Machines and Syst., Beijing, China, Nov. 2003, pp. 153-157.

[14] Y.G. Guo, J.G. Zhu, P.A. Watterson, W.M. Holliday, and W. Wu, "Improved design and performance analysis of a claw pole permanent magnet SMC motor with sensorless brushless DC drive," IEEE Int. Conf. Power Electronics and Drive Syst., Singapore, Nov. 2003, pp. 704-709.

[15] P.A. Watterson, "Analysis of six-step 120° conduction permanent magnet drives," *Australasian Uni. Power Eng. Conf.,* Sydney, Australia, 28 Sept. - 1 Oct. 1997, pp. 13-18.

[16] "Aluminum IP54 motors," Brook Crompton Catalogue 1X1800, July 1991.

[17] "FAS T series brushless servomotors," Vickers Catalogue EPC-GB-B-4030, Motor FAS T1 M2 030, 1991.

[18] H. Weh, H. Hoffmann, and J. Landrath, "New permanent magnet excited synchronous machine with high efficiency at low speed", *Proc. Int. Conf. on Electrical Machines*, 1988, pp. 35-40.

CONFERENCE RECORD

OF THE 2004 IEEE INDUSTRY APPLICATIONS CONFERENCE

39TH IAS ANNUAL MEETING

3-7 OCTOBER 2004 SEATTLE

Volume 1

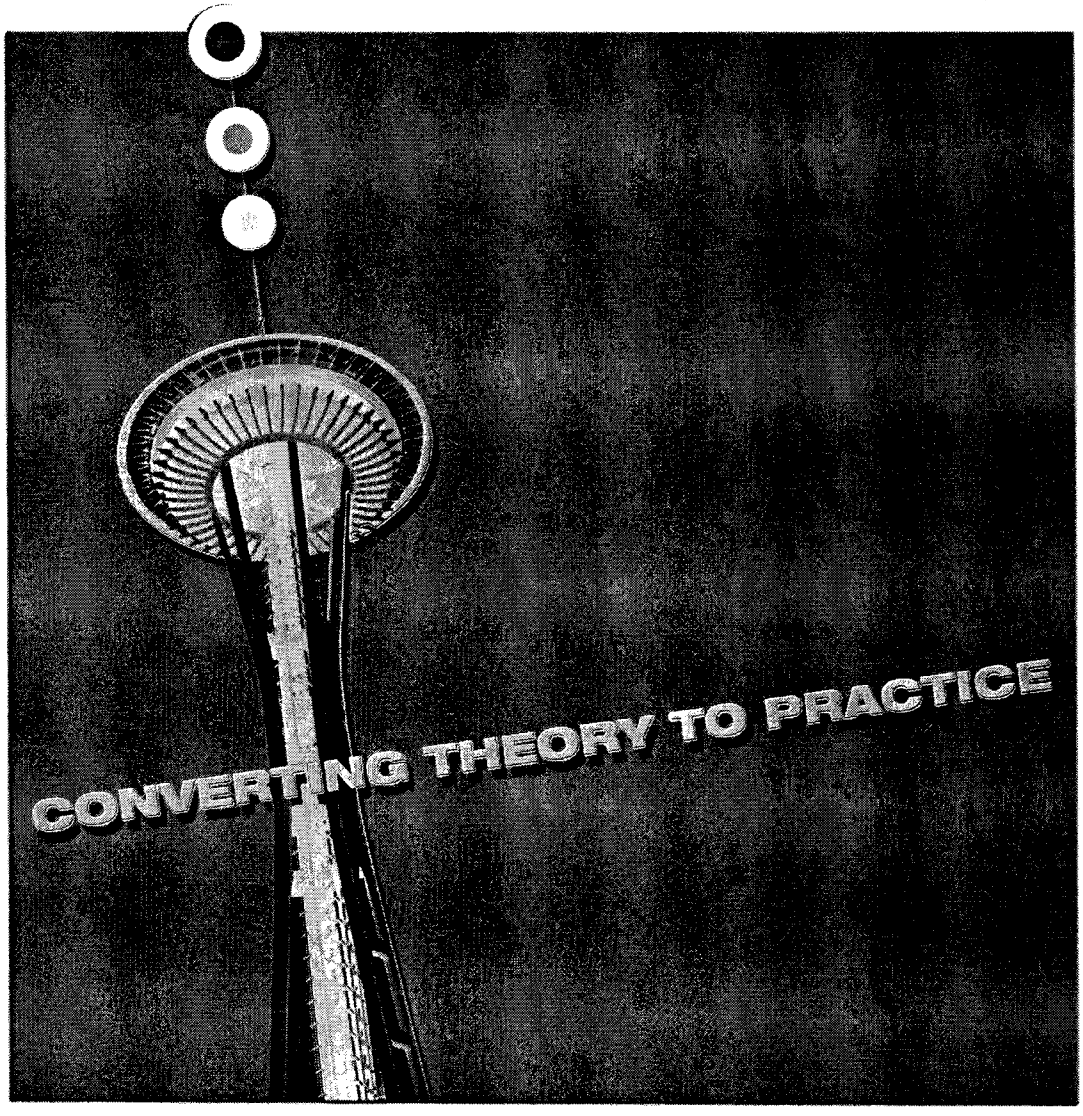

IEEE

IAS IEEE INDUSTRY APPLICATIONS SOCIETY